JOURNAL OF SPACECRAFT AND ROCKETS
Vol. 38, No. 1, January–February 2001

Aerodynamic Heating Measurements on Nose and Elevon of Hypersonic Flight Experiment Vehicle

Keisuke Fujii,* Shigeya Watanabe,† Takuji Kurotaki,‡ and Masao Shirouzu§
National Aerospace Laboratory, Chofu, Tokyo 182-8522, Japan

Aerodynamic heating on the nose and the elevon of the hypersonic flight experiment vehicle was measured using a newly developed sensor, which was calibrated at the heating level corresponding to the level at the real flight condition by a lamp heating test. The calibration test result shows that the sensor could be applicable to the present flight environment. The results of the aerodynamic heating measurements on the nose and the elevon of the vehicle were compared with predictions based on cold hypersonic wind-tunnel tests and computational fluid dynamics (CFD) calculations. The flight-test results on the stagnation region at around t = 100 s were lower than the predictions based on the wind-tunnel tests. The comparisons with CFD results assuming either a fully catalytic wall or noncatalytic wall indicate that the discrepancy could be due to the real gas effect and might be explained qualitatively. For the measurements on the elevon, an increase in aerodynamic heating caused by boundary-layer transition was observed just before it was observed on the windward fuselage.

Nomenclature

h	=	altitude, km, or enthalpy, J/kg
L	=	fuselage length of the vehicle, 4.0 m
M	=	Mach number
Pr	=	Prandtl number of the air, 0.72
p	=	pressure, Pa
q	=	heating rate, kW/m^2
R_{nose}	=	radius of curvature of carbon/carbon nose cap, m
$R_{\text{TC/CC}}$	=	thermal contact resistance between thermocouples and the sensor module
St	=	Stanton number
$\overline{St}$	=	Stanton number ratio, St/St_{ref}
s	=	coordinate along the wall
T	=	temperature, K
T_i	=	ambient temperature, assumed to be 273.15 K
t	=	time after the vehicle separation, s
u	=	flow velocity, m/s
V	=	vehicle velocity, km/s
x, y, z	=	vehicle coordinates; Fig. 5
α	=	angle of attack, deg
γ	=	catalytic efficiency
δ_{elevon}	=	elevon deflection angle, deg, trailing edge down positive
ε	=	emissivity
μ	=	viscosity, kg/m s
ρ	=	density, kg/m^3
σ	=	Stefan–Boltzmann constant, or standard deviation

Subscripts

e	=	value at the edge of the boundary layer at stagnation point
ref	=	reference value
s	=	stagnation value
w	=	wall surface value
0	=	freestream reservoir condition
∞	=	freestream value

Presented as Paper 2000-0267 at the AIAA 38th Aerospace Sciences Meeting, Reno, NV, 10–13 January 2000; received 4 February 2000; revision received 1 August 2000; accepted for publication 3 August 2000.

*Researcher, Space Project and Research Center; keisuke@nal.go.jp. Member AIAA.
†Head, Aero-Thermodynamics Laboratory, Aerodynamics Division; shigeyaw@nal.go.jp. Member AIAA.
‡Senior Researcher, Space Project and Research Center; kurotaki@nal.go.jp. Member AIAA.
§Leader, HOPE-X Management Group, Space Project and Research Center; shiro@nal.go.jp. Senior Member AIAA.

Introduction

IN the design of a high-performance hypersonic lifting vehicle, such as a reentry vehicle, it is necessary to predict its aero- and aerothermodynamic characteristics accurately. The dissociation of the air is one of the most important phenomena. It is still not well understood and has a significant effect on aerodynamic heating of a stagnation region of a reentry vehicle. The phenomenon has been mainly studied on the ground by using high-enthalpy wind tunnels and computational fluid dynamics (CFD) techniques. However, the ground facilities cannot completely simulate the flow conditions in the hypersonic flight. Some difficulties also exist in simulating wall temperature distributions and catalytic efficiency of the wall. In CFD analysis, the chemical models are still to be examined. Therefore, flight data are important for the evaluation of these ground-based tools for estimation of the dissociation effect of the air. Although some flight experiments were conducted[1–3] to acquire aerodynamic heating data in the flight condition to evaluate these prediction methods, flight data are not adequate for complete validations. Thus, the hypersonic flight experiment (HYFLEX) was planned[4] and conducted.[5] The data obtained during the flight of HYFLEX would be effective data for validation. In that flight experiment, aerodynamic heating was measured with the intention of acquiring additional detailed data for the purpose of validating the prediction methods. The aerodynamic heating data on the stagnation region and on the control surface in the flight environment are compared both with the prediction based on wind-tunnel tests and with the nonequilibrium CFD results in this paper.

Integrated heat flux sensors designed for ground facilities, in general, cannot be used in flight measurements in hypersonic speeds, mainly due to higher surface temperatures and longer heating durations compared with a wind-tunnel test. Because the design of sensors for onboard aerodynamic heating measurement is highly dependent on the flight environment, it is necessary to design sensors corresponding to the flight environment, the location of the measurement point, the magnitude and the duration of the heating, and the surface material at the measurement point.[6] For such sensors in flight applications, the relation between incident heat flux and the resulting temperature is not simple, and a mathematical thermal model is necessary to derive the heat flux from the measured temperature. A mathematical thermal model must be constructed based on a calibration test to derive an aerodynamic heating rate from its output temperature within the required accuracy. To measure aerodynamic heating on the nose and elevon of HYFLEX, an aerodynamic heating sensor was developed, and the mathematical thermal model of it was calibrated and tuned by lamp heating tests.

Flight Experiment

The HYFLEX vehicle was launched from the Tanegashima Space Center of the National Space Development Agency of Japan (NASDA) by a two-stage launcher and separated from the launcher at an altitude of 107 km and a velocity of 3.88 km/s. It flew along the path[7] shown in Figs. 1–3. At first, the vehicle kept a constant angle of attack of 49 deg. After experiencing a peak aerodynamic heating (Fig. 4), the vehicle decreased the angle of attack to 30 deg and started an equilibrium glide.

The vehicle had a lifting body shape of 4.40 m in length, 1072.9 kg in total mass, and 0.4 m in nose radius, as shown in Fig. 5. The thermal protection system consisted of a carbon/carbon (C/C) hot structure for nose and elevon, thermal protection system (TPS) ceramic tiles for the lower fuselage and a stabilizing fin, and flexible surface insulations for the upper fuselage, as shown in Fig. 5.

The onboard measurements were conducted as planned, and the data were obtained through telemetry. As shown in Fig. 5, aerodynamic heating was measured at 21 points on the vehicle: 8 points in the C/C region, 11 points in the TPS ceramic tile region, and 2 points in the flexible surface insulation region. In this paper, results of the measurements in the C/C region are presented (TA01–TA17 in Fig. 5). The aerodynamic heating measurements in the TPS ceramic tile region were reported.[8] Radiation from the C/C nose cap rear surface was also measured by a radiometer installed on the bulkhead as shown in Fig. 6 to define the boundary conditions at the rear surfaces of the sensors on the nose cap.

In general, it is better for surface heating measurements in flight experiments to design the sensor by using the same material as the surrounding surface for several reasons. One reason is not to disturb the surrounding surface temperature distribution and another is to withstand the high temperature during flight. It is reported that a mismatch in the surface temperature distribution can lead to

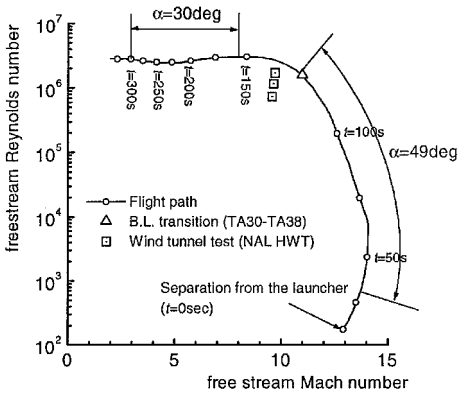

Fig. 1 HYFLEX flight trajectory (Reynolds number–Mach number).

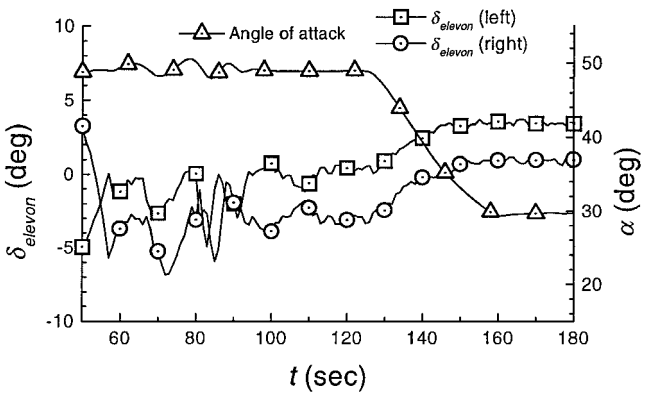

Fig. 2 Angle of attack and elevon deflection angle in HYFLEX flight.

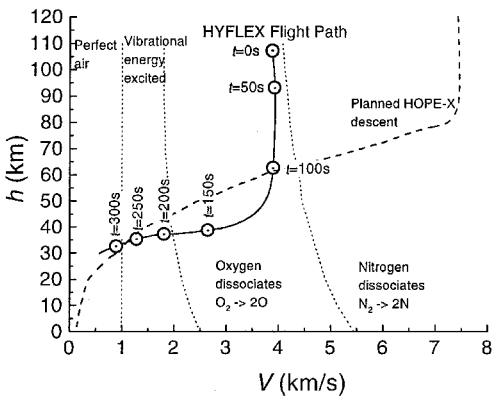

Fig. 3 HYFLEX flight trajectory (*h*–*V*).

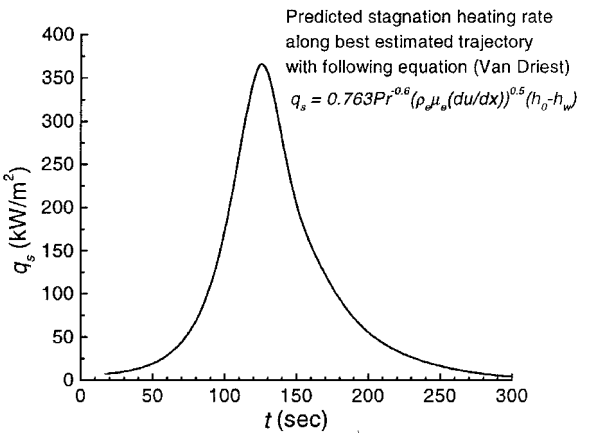

Fig. 4 Predicted aerodynamic heating at the stagnation point.

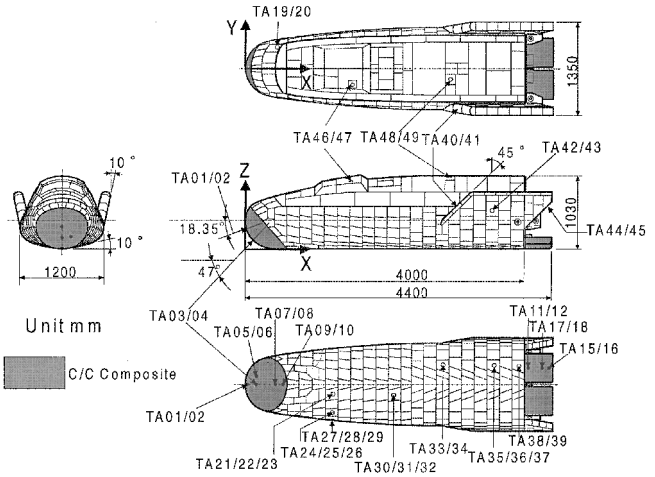

Fig. 5 HYFLEX vehicle configuration and location of aerodynamic heating sensor.

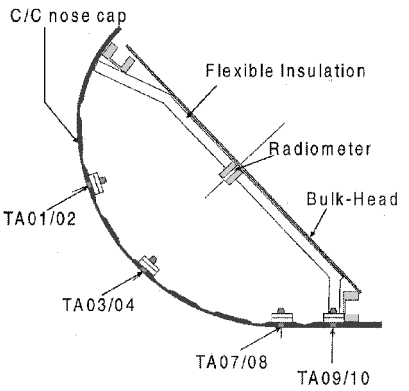

Fig. 6 Sensor locations at the nose cap.

considerable error.[6] Because quantitative correction for this effect in the hypersonic reentry environment is difficult, it is desired that the sensor used in a flight test have as small a heat capacity as possible so as not to disturb the temperature distribution.

Because the predicted stagnation heating rate, assuming wall temperature in balancing between radiation and aerodynamic heating, varies significantly along HYFLEX flight trajectory (Fig. 4), it was taken into consideration that the temperature response at the rear surface of the C/C structure is delayed and that a temperature measurement on the rear surface would make it difficult to reconstruct the input heating rate with the required time response. It was then decided that the temperature measuring point should be close to the outer surface, so that it would provide a good response in the flight test. A plug-in-type sensor was chosen in the present case to avoid the risk in installing thermocouples directly into the nose cap, to facilitate a calibration test, and to take advantage of replacing a possible malfunctioning sensor.

Aerodynamic Heating Sensor

Structure and Specifications of the Sensor

Although the surface temperature is the most important parameter for the derivation of the heating rate, it is also important to estimate correctly the temperature field in the sensor module. For this purpose, each sensor had two thermocouples: One was very close to the surface (0.5 mm in depth), and the other was located 9.0 mm from the surface. A schematic of the sensor is shown in Fig. 7. The sensor module, which is 42.5 mm in length and 20.0 mm in diameter, was fixed to the C/C structure (nose cap or elevon) by a stopper (C/C). A spring (inconel718) was inserted between the stopper and the module to absorb thermal stress. A ceramic washer was inserted to protect the spring from the high temperature during flight. R-type sheathed thermocouples [platinum–13% rhodium(+) vs platinum(−)], platinum sheath diameter of ϕ1.0 mm, were installed in the module and the gaps between the thermocouples and the module and were filled with MgO powder to ensure thermal contact. Because the C/C composite has poor strength for tension in the direction normal to the layer, the nose cap structure of 4 mm in thickness may not be able to sustain the C/C sensor module. Thus, the nose cap structure is padded up to a thickness of about 8 mm in a circular area of 50–80 mm in diameter around the sensor.

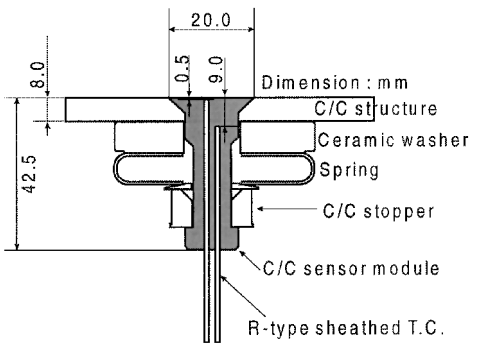

Fig. 7 Structure of C/C aerodynamic heating sensor.

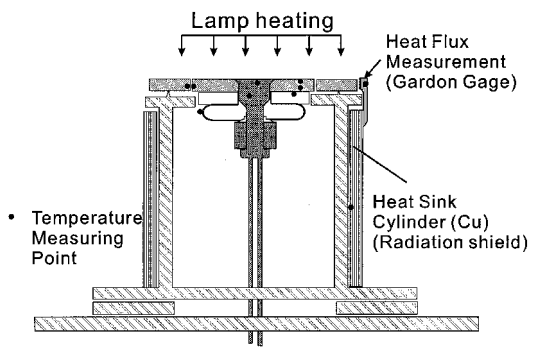

Fig. 8 Setup at the calibration test of the C/C sensor.

Calibration Test for the C/C Sensor

A calibration test was conducted to confirm the validity of the mathematical thermal model. Constructing a mathematical thermal model only from measured parameters may cause differences between the calculated temperature with the model and the measured temperature in the calibration test, such as thermal properties and contact resistances. There are too many uncertain parameters in the thermal model for this C/C sensor. Therefore, it is necessary to select parameters to be tuned, which strongly affect the derivation of the heat flux. On the other hand, parameters that were not taken into account in tuning the model, such as sensor individual differences, errors dependent on heat flux history, or other errors, may affect the heat flux derivation accuracy. To understand such errors, data of another set of heating tests for each sensor, which do not appear here, were utilized. Furthermore, because the unselected parameters also may affect the determination for the parameter tuning itself, the tuned values of parameters in the model may not coincide with their actual values. Accordingly, the calibration test should be conducted under conditions as close to those in flight as possible.

To acquire data for constructing the model, a series of lamp heating tests of the sensor were conducted with a 30-kW Xe-lamp heater in the Japan Ultra-High Temperature Materials Research Center (Fig. 8). In the tests, a sensor module that was installed in a ϕ60 mm C/C panel representing the nose cap or elevon of the HYFLEX was heated with a steplike heating pattern, and the temperature histories were recorded. The incident heat flux by the lamp, ranging around 250 kW/m^2, was measured with a calibrated Gardon-type heat flux transducer during the test. The bottom half of the sensor structure was surrounded by a black-painted cylindrical heat sink to reduce radiative interaction, and the temperature of the heat sink was measured during the test to confirm the rear side boundary condition.

Mathematical Thermal Model for Calibration Tests

In the thermal analysis of the calibration tests, an axisymmetric two-dimensional finite difference method was used. The sensor elements were represented in a grid shown in Fig. 9. Incorporating a sensor module, a C/C panel, a ceramic washer, a spring, and a platinum-sheathed thermocouple, two thermocouples were represented by one thermocouple in the model for simplicity. Temperature dependency of the contact thermal resistance between the sensor module and the C/C panel was assumed, which was determined based on independent measurements of the resistance with changing temperature and the contact pressure.

The surface temperature was estimated by iteration so that the calculated temperature at the sheathed thermocouple agrees with the measurement. A uniform incident heat flux distribution was assumed as the surface boundary condition in the iterative calculation. The rear side of the sensor was assume to encounter a blackbody emission at temperature of 273.15 K because the cylindrical heat sink surrounding the sensor was painted black and the temperature rise was small. Thermal properties of components of the sensor and

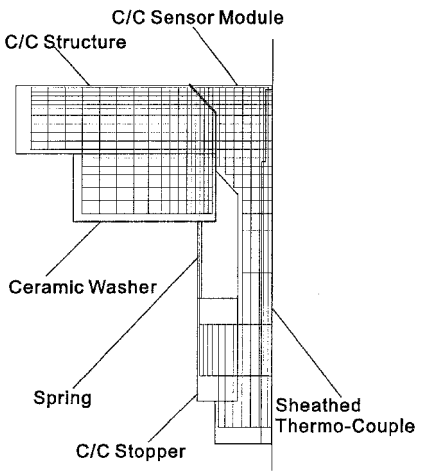

Fig. 9 Grid for the sensor analysis.

Table 1 Thermal properties of the C/C materials used in the sensor

Thermal property	Temperature, °C 25	500	1000	1500
C/C composite 1: C/C structure (nose cap, elevon surface)				
Specific heat C, J/kg K	666	1327	1817	2277
Thermal conductivity κ, W/mK				
Horizontal	20.49	33.91	34.87	43.53
Vertical	4.552	7.535	7.744	9.67
Emissivity, ε	0.85	0.85	0.85	0.85
C/C composite 2: C/C sensor module, C/C stopper				
Density ρ, kg/m^3	1867.2	1867.2	1867.2	1867.2
Specific heat C, J/kg K	785	1733	2157	2416
Thermal conductivity κ, W/mK	121.9	114.7	92.11	72.07
Emissivity, ε	0.87	0.87	0.87	0.87

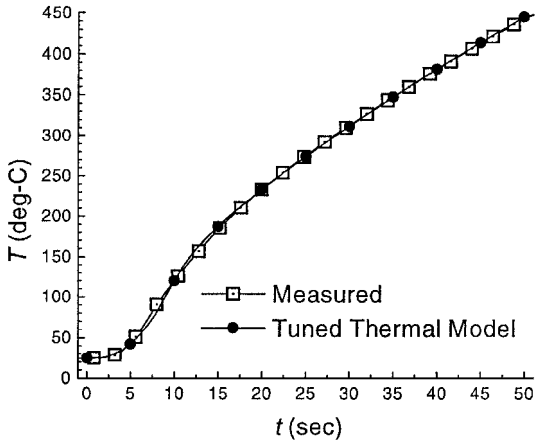

Fig. 10 Thermal model tuning by calibration test.

thermal contact resistance used in the thermal analysis are shown in Table 1.

Mathematical Thermal Model Tuning

The comparison between the measured temperature of the sensor module in the calibration test and the calculated temperature of the model is shown in Fig. 10. Tuning only the thermal contact resistance between the sensor module and the sheathed thermocouple as a function of temperature whose value was not measured independently, the mathematical thermal model came to agree with the calibration test results using measured values for all other thermal properties, emissivity of each element, and thermal contact resistance between them. With the tuned mathematical thermal model, the calculated temperature history at the thermocouple point from the measured heat flux agrees well with the measured temperature, as shown in Fig. 10. Figure 10 shows that the mathematical thermal model is valid for calculating aerodynamic heating. The overall errors, including the errors in estimating heat flux based on this model and the errors due to deviation among individual sensors, which were estimated from a separate calibration test conducted for all onboard sensors in the HYFLEX vehicle, are about 5.7% in total at a heating rate of approximately 250 kW/m^2. Because no reliable calibration data at the heating rate below 250 kW/m^2 were acquired at this time, the error is an assumed constant heating rate in that range, which, consequently, means a larger error ratio in lower heating rate conditions.

Flight Data Processing

With the mathematical thermal model just described, the aerodynamic heating in the flight was derived from the measured temperature history. Both heating rate and surface temperature were determined by iterations so that calculated temperature at the thermocouple point agrees with the measurement. The grid and the procedure in the flight data analysis were identical to that for the calibration test, except that the grid for the flight included the pad-up of the C/C panel, and the heat flux to the surface was assumed uniform in Stanton number instead of heat flux.

One important difference between the flight and the calibration is that a strong emission and reflection may come from the bulkhead to the rear surface of the sensor in flight. In the flight situation, the magnitude of the radiation varies with time, as well as with location of the sensor and with direction. To take this into account, temperature distribution of the bulkhead and resultant radiation fields were calculated for each time step and were set as the rear side boundary condition in the sensor analysis using the thermal model. Temperature of the C/C nose cap and of the surface of the bulkhead insulation were calculated with three-dimensional and one-dimensional finite difference methods, respectively. Aerodynamic heating was assumed from the reference Stanton number[9] [Eq. (1)] and Lees's distribution.[10] The radiation field is calculated with a time step of 0.5 s. Onboard measurement of the a commercially calibrated radiometer installed on the bulkhead insulation are utilized to estimate the amount of error concerning the rear boundary condition.

The elevon structure is too complicated for an accurate estimate the radiative boundary condition, and neither the temperature at the upper surface nor radiation inside the elevon were measured in the flight. Therefore, two limiting cases were assumed as one of the error sources in the elevon sensor analysis, as follows: 1) the rear side of the sensor emits radiation of $\varepsilon\sigma T^4$ and encounters no other radiation than σT_i^4 ($T_i = 273.15$ K) and 2) all radiation emitted from the rear side of the sensor reflects directly (insulated).

Aerodynamic heating data are compared as a Stanton number $\overline{St}$ normalized by the reference Stanton number at the stagnation point of a nose radius of 0.4 m in a perfect gas assumption, St_{ref} (Ref. 9)

$$\overline{St} = St/St_{\text{ref}}$$

where

$$St = \frac{q_s}{\rho_\infty \mu_\infty (h_0 - h_w)}, \qquad St_{\text{ref}} = \frac{0.763 Pr^{-0.6}\sqrt{\rho_e \mu_e (\mathrm{d}u_e/\mathrm{d}s)}}{\rho_\infty \mu_\infty}$$

$$\frac{\mathrm{d}u_e}{\mathrm{d}s} = \frac{1}{R_{\text{nose}}}\sqrt{\frac{2(p_e - p_\infty)}{\rho_e}} \tag{1}$$

In the comparison using the Stanton number ratio, errors from estimation of freestream properties should be considered. The estimation of freestream conditions,[11] such as static temperature and static pressure, are based on data observed by National Oceanic and Atmospheric Administration polar satellites. The error in the estimation was determined by comparing the meteological rocket data with an estimation based on the identical procedure and is shown in Table 2. The estimation error of wind velocity in Table 2 is an assumed value. Errors in Stanton number ratio $\overline{St}$ due to the estimation error of freestream conditions are expected to be about 4.6%. All errors just described are summarized in Table 3 in Stanton number $\overline{St}$, showing that the C/C sensor can be applicable to the HYFLEX flight measurement purpose. Note that these estimations of the magnitude of errors are valid only for $t < 120$ s for the nose cap and $t < 130$ s for the elevon because after that the temperatures of the elements of the sensor become high compared with those during the calibration tests, and the mathematical thermal model would be no longer valid under such temperature distribution.

Table 2 Assumed estimation error of freestream condition

Parameter	Estimation error
Static temperature	5 K
Static pressure	3%
Relative velocity	50 m/s[a]

[a]Assumed value based on the maximum wind velocity along the flight path calculated with GRAM-90 (Ref. 7).

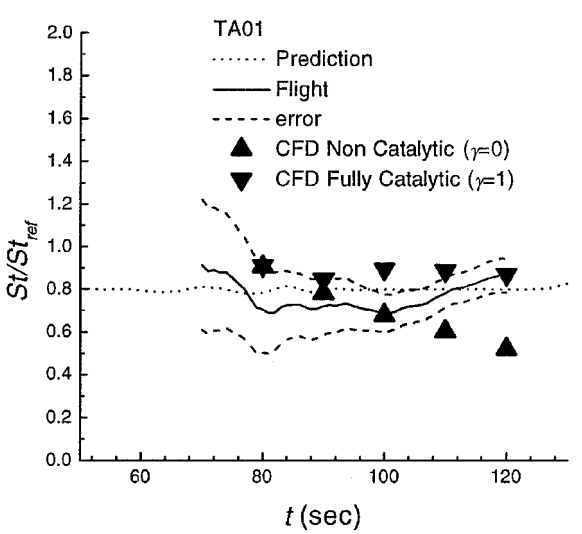

a) TA01 (x = 20 mm, y = 0 mm, z = 274 mm)

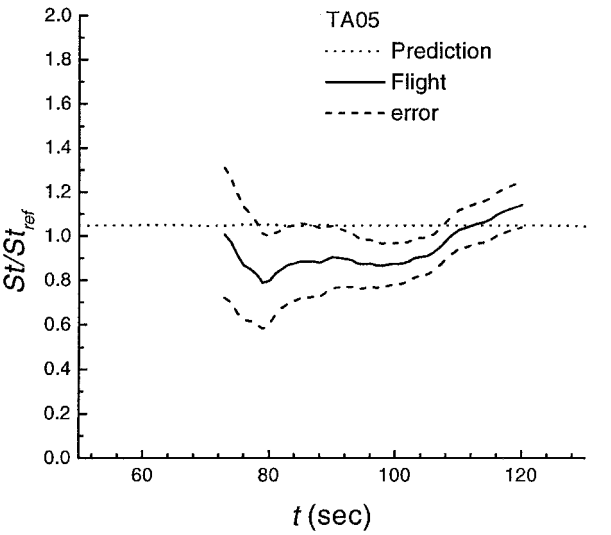

c) TA05 (x = 136 mm, y = −99 mm , z = 117 mm)

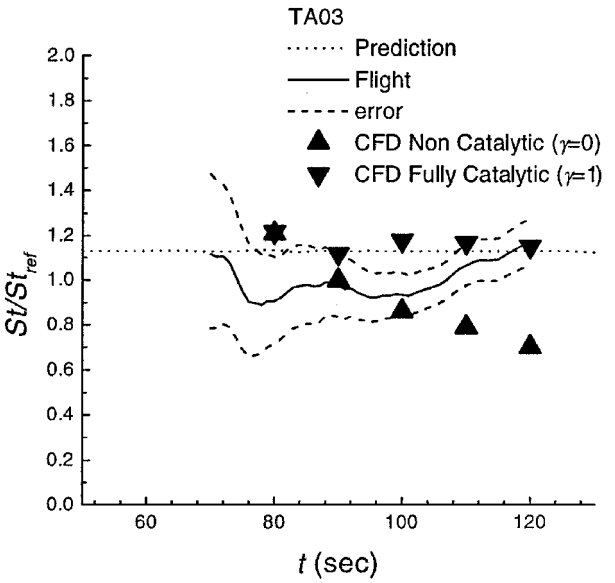

b) TA03 (x = 127 mm, y = 0 mm, z = 107 mm)

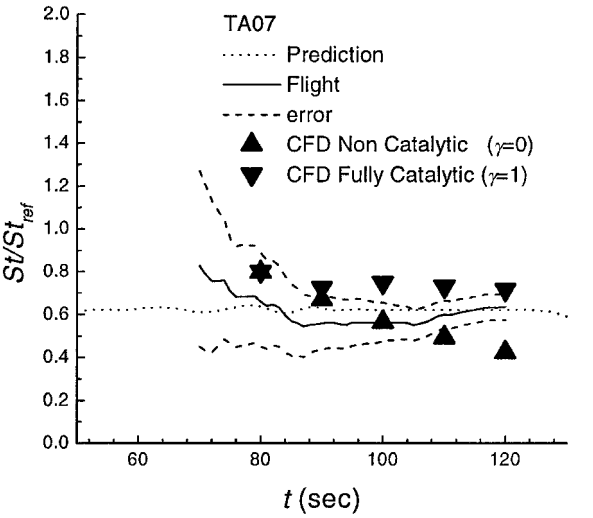

d) TA07 (x = 400 mm, y = 0 mm, z = 0 mm)

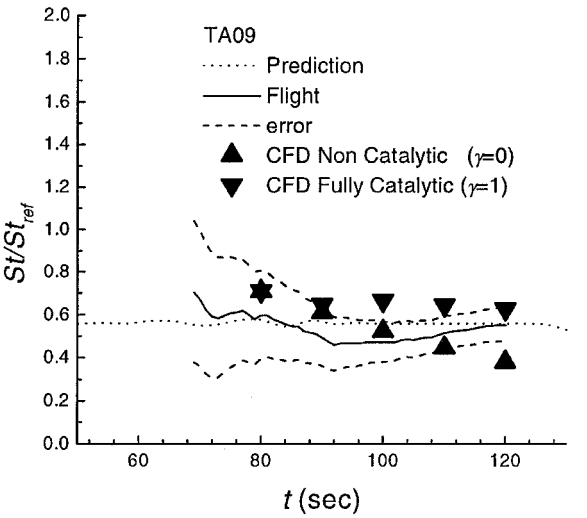

e) TA09 (x = 500 mm, y = 0 mm, z = 0 mm)

Fig. 11 Stanton number ratio at the nose in flight.

Table 3 Accuracy of the heat flux measurement with the C/C sensor

Parameter	σ_{St/St_0}
Error of thermal model (RSS), $q < 250$ k W/m^2	0.057
Lamp heating accuracy	0.047
Disagreement with the model	0.030
Individual differences	0.019
Effect of rear side boundary condition (max)	0.124[a]
Estimation of freestream condition (max)	0.046
Temperature mismatch effect (max.)	0.054[b]

[a]Difference in the effect between the two limiting cases, not standard deviation.
[b]Estimation values[8] (not taken into account in Figs. 11 and 14 in this paper).

Note the effect of a surface temperature mismatch between the sensor module, the pad-up part (8 mm thick), and the C/C general part (4 mm thick). The temperature mismatch became about 400 K at maximum in the nose case due to heat capacities of the sensor components, such as the module and the pad-up. Although this effect is difficult to estimate accurately, estimation by the method of Westkaemper[12] shows the effect would be within 5.4% in the worst case.

Flight Results and Discussion

Ground-Based Aerodynamic Heating Prediction

Wind-tunnel test data for comparison were obtained at the cold hypersonic wind tunnel of the National Aerospace Laboratory of Japan. The test was conducted with a 10% scale model of the HYFLEX vehicle, which had heat flux gauges at the locations corresponding to the sensors in the vehicle. The freestream Mach number was approximately 9.6, and the freestream Reynolds number based on the fuselage length ($L = 4.0$ m) ranged from 6.7×10^5 to 1.6×10^6, as shown in Fig. 1. Because of its low Reynolds number, the boundary layer on the whole model surface was laminar in the test. Predicted heating rates in this paper are reduced, considering only the effect of angle of attack and assuming neither Mach number effect nor enthalpy effect.

On the other hand, CFD calculations around the nose of the HYFLEX vehicle with three-dimensional nonequilibrium Navier–Stokes code were conducted along the flight trajectory to compare directly with the flight data. This code, which was previously validated with experiments and other numerical codes, is described in Ref. 13. Because aerodynamic heating in chemically nonequilibrium flow depends strongly on the wall catalycity, the calculations were conducted in two limiting cases: 1) a fully catalytic wall case and 2) a noncatalytic wall case. Wall temperature on the whole vehicle was assumed for simplicity to be equal to the temperature measured at TA03 in the calculations. TA03 is located close to the stagnation point at an angle of attack of 49 deg. The details of the code are shown in Table 4 (Refs. 14 and 15).

Flight Data and Comparison with Predictions

Stanton number ratios at each sensor in the flight are shown in Figs. 11a–11e (solid line), along with the error (dashed line), which includes not only sensor errors but also that which comes from freestream estimation as shown in Table 3. In Figs. 11, the dotted lines indicate the prediction based on the wind-tunnel test data, in which only the angle of attack effect on $\overline{St}$ was taken into account. CFD results for the fully catalytic wall and for noncatalytic wall are indicated with symbols ▼ and ▲, respectively, at the sensor in the symmetric plane (TA01, TA03, TA07, and TA09). Because the error of Stanton number $\overline{St}$ earlier than $t = 70$ s is large due to low heat flux level, only the data after $t = 70$ s are shown in Figs. 11. However, at around $t = 80$ s, the error is so large that any meaningful results cannot be seen. The flight data for TA03, for example, indicate a lower heating rate than the prediction around $t = 100$ s, and then flight heating data approach the prediction. This tendency can be seen in all sensors on the nose cap.

One possible reason for the discrepancy with the prediction around $t = 100$ s is the effect of dissociation of the air. CFD results for the fully catalytic wall (symbol ▼) and the noncatalytic wall (symbol ▲) disagree with each other after about $t = 90$ s, and a substantial difference can be seen at around $t = 100$ s. The flight data seem to agree with the noncatalytic result at around $t = 100$ s and vary toward the fully catalytic result after $t = 100$ s. This tendency can be qualitatively explained by the effect of surface temperature increase, as follows: It is known that catalytic efficiency γ of SiO_2-based coating, which is formed by the oxidation of SiC coating, increases on O_2 and N_2 dissociation with surface temperature. The result shown in Fig. 11b is replotted surface-temperature-wise ($1000/T$) in Fig. 12. The flight data digress from noncatalytic CFD results at around 500 K and agree with fully catalytic results at around 800 K, which is consistent with the surface temperature dependency of catalytic efficiency of O_2 recombination shown in Fig. 13 (Refs. 16–18), though this tendency is still unclear quantitatively. Although further study, such as CFD calculations with a finite catalytic efficiency model, should be done, it is shown that the variation in $\overline{St}$ can be qualitatively explained by the effect of dissociation of the air and by surface temperature dependency of the catalycity. Prior to $t = 100$ s, though flow is a dissociated and nonequilibrium one according to CFD calculations, the difference between the fully catalytic case and the noncatalytic case is very small.

The flight results of aerodynamic heating at the elevon shown in Fig. 14 are characterized by a sharp increase in $\overline{St}$ at about $t = 120$ s. The timing when the sharp increase was observed is earlier than

Table 4 Details of the nonequilibrium analysis code

Parameter	Model
Convective term	AUSM+ scheme[14]
Gas model	7 species, 18 reactions
Reaction physical model	Park's two-temperature model[15]

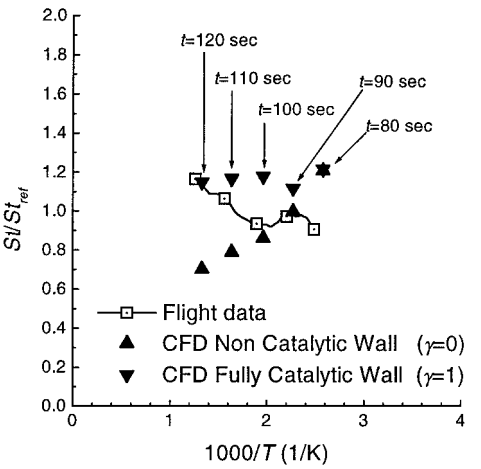

Fig. 12 Temperature dependency at TA03.

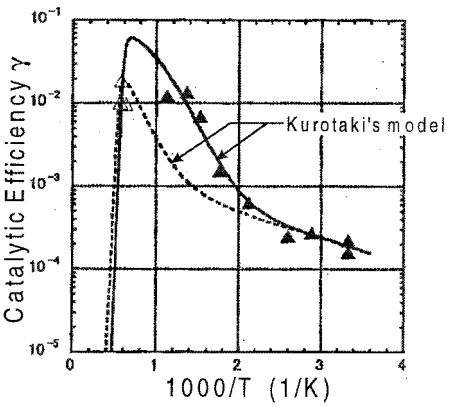

Fig. 13 Temperature dependency of catalytic efficiency for O_2–O mixtures gas: ▲, Greaves and Linnett[17] (silica, p_e = 14.7–16.0 Pa); △, Kolokziej and Stewart[18] (RCG, p_e = 412.0 Pa); ——, present model (p_e = 15.3 Pa)[16]; and – – –, present model (p_e = 410 Pa).[16]

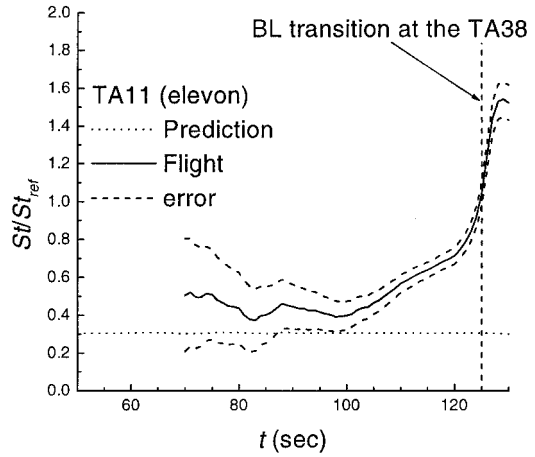

TA11 (x = 4050 mm)

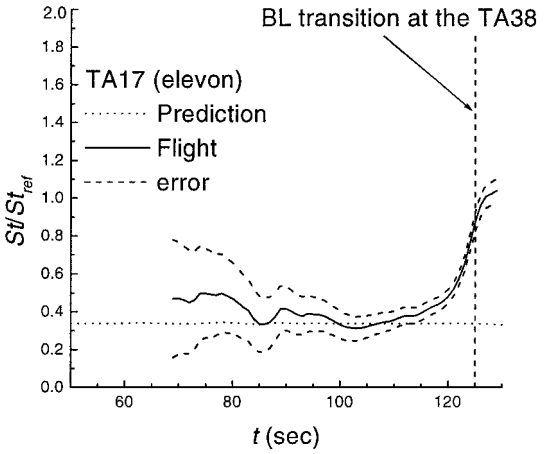

TA17 (x = 4240 mm)

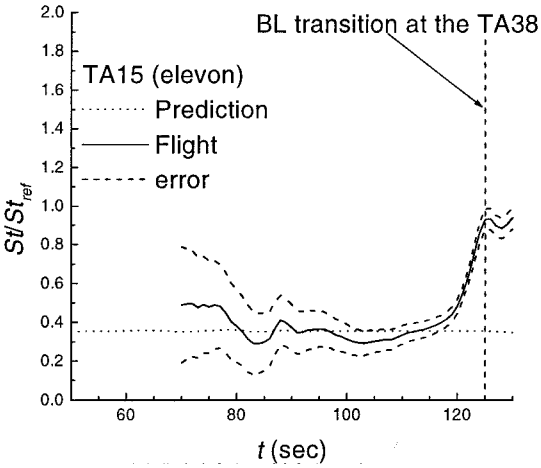

TA15 (x = 4337 mm)

Fig. 14 Stanton number ratio at the elevon in flight.

when the boundary-layer transition was observed in the windward fuselage at $t = 126$ s (Ref. 8). It can be concluded that the sharp increase was caused by boundary-layer transition. Another tendency that can be seen in the figures is that the heating rate increases gradually from the prediction before the boundary-layer transition. The discrepancy from the prediction becomes smaller as it goes downstream (from TA11 through TA17 to TA15). The discrepancies before $t = 120$ s cannot be explained by boundary-layer transition or Reynolds number effect on separation. Also, temperatures around the sensors are so low that the estimation error for radiation behind the elevon has little influence on the heat flux derivation at the time. The reason for this discrepancy is not known.

Conclusions

Aerodynamic heating on the nose and the elevon of the HYFLEX vehicle were measured by using newly developed C/C aerodynamic heating sensors. These sensors were calibrated by lamp heating tests intended to provide high-accuracy measurements, and a mathematical thermal model of them was constructed based on the results in the calibration tests. The calibration test results show that the sensor could be applicable to the present flight environment.

The results of the aerodynamic heating measurements on the nose and the elevon of the vehicle were compared with predictions based on a cold hypersonic wind-tunnel tests and CFD calculations. The flight-test results were lower than the predictions based on the wind-tunnel tests on the stagnation region at around $t = 100$ s. The comparisons with CFD results assuming either a fully catalytic wall or a noncatalytic wall indicate that the discrepancy could be due to the effect of dissociation of the air and might be explained by the dependency of catalycity on the surface temperature qualitatively.

For the measurements on the elevon, an increase in aerodynamic heating caused by boundary-layer transition was observed just before it was observed on the windward fuselage.

References

[1]Curry, D. M., Rochelle, W. C., Chao, D. C., and Ting, P. C., "Space Shuttle Orbiter Nose Cap Thermal Analysis," AIAA Paper 86-0388, Jan. 1986.

[2]Throchmorton, D. A., "Benchmark Determination of Space Shuttle Orbiter Entry Aerodynamic Heat-Transfer Data," *Journal of Spacecraft and Rockets*, Vol. 20, No. 3, 1983, pp. 219–224.

[3]Hodge, J. K., and Audley, D. R., "Aerothermodynamic Parameter Estimation from Space Shuttle Thermocouple Data During Transient Flight Test Maneuvers," AIAA Paper 83-0482, Jan. 1983.

[4]Shirouzu, M., and Watanabe, S., "On the Hypersonic Flight Experiment (HYFLEX) for the Development of HOPE," AIAA Paper 93-5080, Nov. 1993.

[5]Shirouzu, M., Watanabe, S., and Suzuki, H., "A Quick Report of the Hypersonic Flight Experiment, HYFLEX," International Symposium on Space Technology and Science, Paper 96-f-09, May 1996.

[6]Neumann, R. D., Erbland, P. J., and Kretz, L. O., "Instrumentation of Hypersonic Structures," AIAA Paper 88-2612, June 1988.

[7]Suzuki, H., Ishimoto, S., and Morito, T., "Postflight Evaluation of the HYFLEX Guidance, Navigation, and Control," AIAA Paper 96-4525, Nov. 1996.

[8]Fujii, K., and Inoue, Y., "Aerodynamic Heating Measurement on Afterbody of Hypersonic Flight Experiment," *Journal of Spacecraft and Rockets*, Vol. 35, No. 6, 1998, pp. 736–741.

[9]Van driest, E. R., "The Problem of Aerodynamic Heating," *Aeronautical Engineering Review*, Vol. 15, No. 10, 1956, pp. 26–41.

[10]Lees, L., "Laminar Heat Transfer over Blunt-Nosed Bodies at Hypersonic Flight Speeds," *Jet Propulsion*, Vol. 26, No. 4, 1956, pp. 259–269, 274.

[11]Shirouzu, M., Suematsu, S., and Yamamoto, H., "Estimation of the State of the Atmosphere Using NOAA Polar Satellite Data," National Aerospace Lab., NAL-TM-700, Tokyo, July 1996 (in Japanese).

[12]Westkaemper, J. C., "On the Error in Plug-Type Calorimeters Caused by Surface-Temperature Mismatch," *Journal of the Aerospace Sciences*, Vol. 28, No. 11, 1961, pp. 907, 908.

[13]Kurotaki, T., and Yamamoto, Y., "Axisymmetric and Three Dimensional Non-equilibrium Hypersonic Flow Analysis Around Re-Entry Vehicles," International Symposium on Space Technology and Science, Paper 98-d-18, 1998.

[14]Liou, M. S., "A Sequel to AUSM: AUSM+," *Journal of Computational Physics*, Vol. 129, No. 2, 1996, pp. 364–382.

[15]Park, C., *Nonequilibrium Hypersonic Aerothermodynamics*, Wiley, New York, 1990, pp. 89–118.

[16]Kurotaki, T., "Construction of Catalytic Model on SiO_2-Based Surface and Application to Real Trajectory," AIAA Paper 2000-2366, June 2000.

[17]Greaves, J. C., and Linnett, J. W., "Recombination of Atoms at Surfaces, Part 6—Recombination of Oxygen Atoms on Silica from 20°C to 600°C," *Transactions of the Faraday Society*, Vol. 55, 1955, pp. 1355–1361.

[18]Kolodziej, P., and Stewart, D. A., "Nitrogen Recombination on High-Temperature Reusable Surface Insulation and the Analysis of Its Effects on Surface Catalysis," AIAA Paper 87-1637, 1987.

T. C. Lin
Associate Editor